



Bi-objective optimisation based tuning of pressure control algorithms for water distribution networks

Giacomo Galuppini ^{*}, Enrico Creaco, Lalo Magni

Dipartimento di Ingegneria Civile e Architettura, University of Pavia, Pavia 27100, Italy



ARTICLE INFO

Keywords:

WDN
RTC
PI
Smith predictor
Genetic algorithm

ABSTRACT

With the application to water industry of the *Industry 4.0* approach (i.e. the *Water 4.0* approach), Real Time Control is gaining attention as a strategic tool for the management of Water Distribution Networks. Moreover, this approach favours the installation of a wired communication infrastructure, which guarantees new standards in communication between sensors, actuators and control units. This work focuses on the particular task of service pressure regulation, obtained by means of a closed-loop control based on Pressure Control Valves and frequency domain control algorithms. While the topics of the identification of proper control structures, and the analysis of their stability and robustness properties were covered in previous works, this paper is aimed at improving the design phase of such algorithms by formulating the regulator tuning problem as a bi-objective optimisation one. Its solution leads to a Pareto front that captures the typical design trade-off between regulation performances and control effort and robustness, and helps the designer selecting the favoured tunings to be tested on the plant. Simulations performed on a detailed model of two different WDNs highlight the benefits of the approach and the reliability of the obtained tunings.

1. Introduction

Real Time Control (RTC) of service pressure is attracting more and more interest in the context of Water Distribution Networks (WDNs) managements, due to its multiple benefits. As a matter of fact, RTC is an effective way to reduce leakage (Creaco & Walski, 2017; Farley & Trow, 2003) and risk of pipe bursts (Creaco & Walski, 2017; Lambert, Fantozzi, & Thornton, 2013; Thornton & Lambert, 2006). Moreover, RTC algorithms can also be developed to recover energy from WDN turbines or similar devices (Fontana, Giugni, Glielmo, & Marini, 2016; Fontana, Giugni, & Portolano, 2012; Mennemann, Marko, Schmidt, Kemmetmüller, & Kugi, 2019; Pugliese, De Paola, Fontana, Giugni, & Marini, 2016).

While, in the past, the research literature mainly focused on high level, optimal or predictive control algorithms aimed at managing the main WDN components (reservoirs, pumps, valves...) to optimise the overall WDN functioning (Cembrano, Wells, Quevedo, Pérez, & Argelaguet, 2000; Grosso, Maestre, Ocampo-Martínez, & Puig, 2014; Grosso et al.(2014b)Grosso, Ocampo-Martínez, Puig, & Joseph, 2014; Grosso, Velarde, Ocampo-Martínez, Maestre, & Puig, 2017; Ocampo-Martínez, Barcelli, Puig, & Bemporad, 2012; Ocampo-Martínez, Puig, Cembrano, & Quevedo, 2013; Salomons & Housh, 2020; Toro, Ocampo-Martínez, Logist, Impe, & Puig, 2011), a recent research branch moved the attention on low level controllers. Such controllers can be coupled in hierarchical schemes with higher level ones, with the specific task

of service pressure regulation (Campisano, Creaco, & Modica, 2009; Campisano, Modica, Reitano, Ugarelli, & Bagherian, 2016; Campisano, Modica, & Vetrano, 2011; Creaco, Campisano, Fontana, Marini, Page, & Walski, 2019; Fontana, Giugni, Glielmo, Marini, & Verrilli, 2017; Fontana, Giugni, Glielmo, Marini, & Zollo, 2017).

This shift is due to the rise of the *Water 4.0* approach (Hermann, Pentek, & Otto, 2016), i.e. the application to water industry of the wider *Industry 4.0* concept (Sedlak, 2014). WDNs are made *smart*, with the spread of advanced sensors and actuators throughout the whole plant, and their integration in the Industrial Internet of Things (IIoT) network. The *Water 4.0* approach favours the application of users' demand monitoring (Alvisi, Franchini, & Luciani, 2018; Candelieri & Archetti, 2014; Fiorillo, Galuppini, Creaco, De Paola, & Giugni, 2020), fault and leakage detection (Jiménez-Cabas, Romero-Fandiño, Torres, Sanjuan, & López-Estrada, 2018; Kauffeld, 2018), water quality control (Avvedimento, Todeschini, Giudicianni, Di Nardo, Walski, & Creaco, 2020; de Winter, Palleti, Worm, & Kooij, 2019), energy recovery (Fontana, Giugni, Glielmo, Marini, & Zollo, 2020; Mennemann et al., 2019) and, finally, RTC techniques. As a matter of fact, in a scenario where sensors and actuators can be connected by wire (e.g. by means of optical fibre) to the computing units, control algorithms can be based on dynamical models of the plant, and work with sampling times in the order of seconds, as opposed to higher level controllers typically based on static models of the whole WDN, and working at slower rates.

* Corresponding author.

E-mail address: giacomo.galuppini01@ateneopv.it (G. Galuppini).

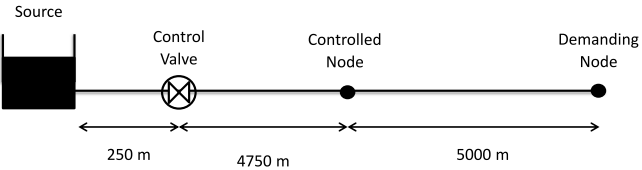


Fig. 1. Case Study A. Topology of the water distribution system (Galuppini et al., 2019).

Recent works focus on the design of frequency domain control algorithms, based on linear models, approximating the WDN dynamics around the working point (Fontana, Giugni, Glielmo, Marini, & Verrilli, 2017; Fontana, Giugni, Glielmo, Marini, & Zollo, 2017; Galuppini, Creaco, Toffanin, & Magni, 2019; Janus & Ulanicki, 2017). Both simulations and field experiments stress the correctness of the approach. More theoretical works analyse stability and robustness of such control schemes, emphasising some important caveats that characterise their design, and providing more advanced solutions to face the problem (Galuppini, Creaco, & Magni, 2020; Galuppini, Magni, & Creaco, 2020; Janus & Ulanicki, 2018). In particular, Galuppini, Creaco et al. (2020) proposes a gain scheduling approach that improves both robustness of the control scheme and its performances. Still, in all the aforementioned works, the nominal design of the regulator is based on a manual loop function design, with the shaping of loop functions obtained with a pole compensation approach applied when possible (Galuppini, Creaco et al., 2020; Galuppini et al., 2019), or with a trial-and error procedure (Campisano et al., 2011; Fontana, Giugni, Glielmo, Marini, & Zollo, 2017; Galuppini, Creaco et al., 2020; Galuppini et al., 2019; Janus & Ulanicki, 2017).

The main goal of this work is instead to propose an optimisation-based approach for the nominal design of the regulator. The design problem is formulated as a bi-objective optimisation one, which encapsulates the main requirements for the closed-loop system, both in terms of robust stability and performance. This approach is preferred to more standard ones, typically based on the design of a target loop function and on the minimisation of some distance among the target function and the actual one (Cominos & Munro, 2002; Gaikwad, Dash, & Stein, 1999; Grassi & Tsakalis, 1996; Tan, Liu, & Tam, 1998), due to the complexity of the process transfer function, as discussed more in detail in the following of this work. Furthermore, a bi-objective approach, which formalises the typical trade-off arising in the design of sensitivity and complementary sensitivity function, does not require any *a priori* preference metric and provides the designer with a set of optimal (in a Pareto sense) tunings that can effectively help choosing the most promising ones to be tested on the plant (Deb, 2001). The effectiveness of the approach is confirmed by simulations performed on a detailed numerical model of two different WDNs (Galuppini et al., 2019). The bi-objective approach to regulator design, which explicitly accounts for two different and contrasting objective functions, and provides the designer with a description of the associated Pareto front, represents a novelty in the field of RTC. However, the bi-objective problem formulation can be easily adapted to other applications that require balance between control performances and cost of control.

This paper is organised as follows: Sections 2 and 3 summarise the two case studies and their numerical model, adopted for simulations; Section 4 summarises the overall control approach, Fig. 7 represents the core of this work and discusses in detail the bi-objective optimisation approach for the regulator design. Results of the novel, optimisation-based tuning phase are reported in Section 6; Section 7 introduces the results obtained with simulations. Section 8 is devoted to the discussion of result, while Section 9 summarises the main findings of this work.

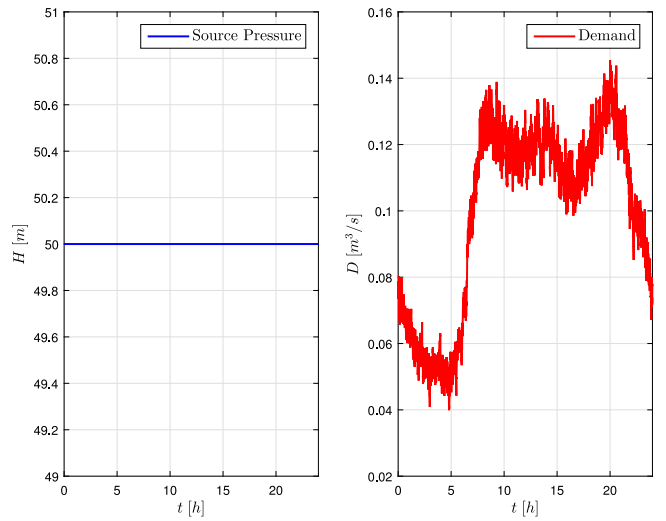


Fig. 2. Case Study A. Source pressure and demand profile.

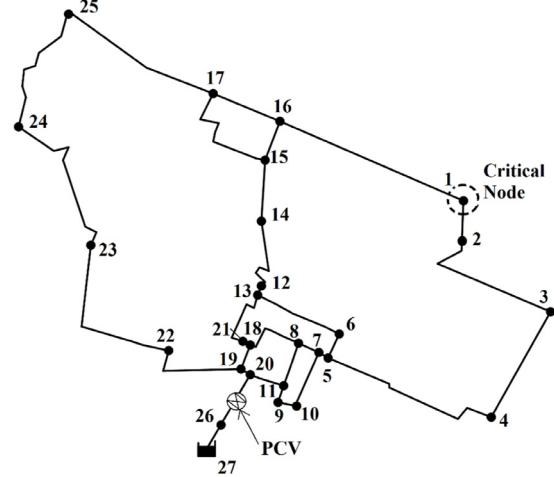


Fig. 3. Case Study B. Topology of the WDN (Creaco, 2017).

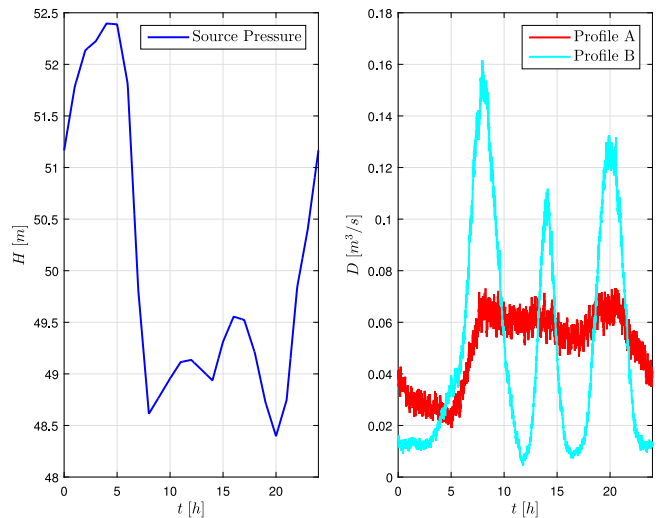


Fig. 4. Case Study B. Source pressure and total demand profiles (sum of nodal demands across the WDN).

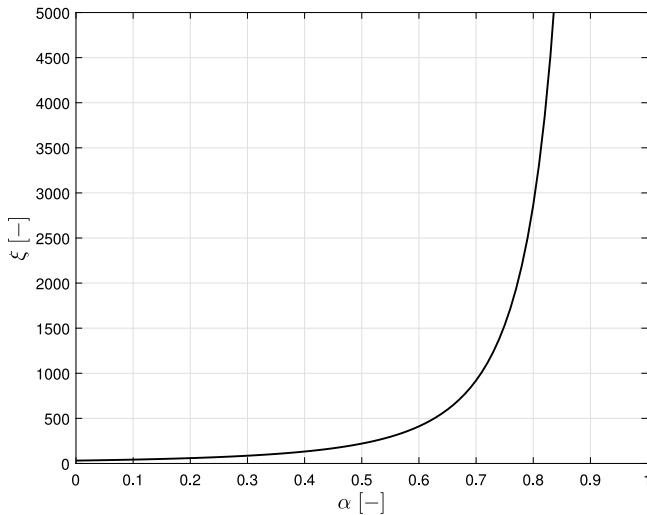


Fig. 5. The local loss coefficient ξ as function of the valve closure α .

2. Case studies

As in Galuppini, Creaco et al. (2020), Galuppini et al. (2019), two different WDN topologies, characterised by very different dynamic behaviours, are adopted as case studies to assess the performances of control algorithms.

Case Study A, depicted in Fig. 1, consists of a simple water distribution system, with a single source node, connected to a single demanding node by means of a pipe. A sensor measures the pressure in the middle of the pipe. Actuation is obtained by means of a pressure control valve (PCV), which is installed 250 m downstream of the source node. The time behaviours of source pressure head and demand are depicted in Fig. 2. Simulations are repeated introducing different offsets ($\{-0.03; 0.05\}$ [m³/s]) in the demand profile, to cover a wider range of operating conditions and account for possible seasonal variation of the demand. No leakage is considered in this system.

Case Study B is represented by the skeletonised WDN of the Italian town of Castelfranco Emilia (about 30,000 inhabitants). Actuation is obtained by means of a PCV installed in pipe 26–20 linking the source to the rest of the network, while pressure is measured at node 1, as depicted in Fig. 3. Two different demand patterns are considered for this case study, leading to two different trends of the total WDN demand (see Fig. 4): a flatter trend (profile A) and a more peaked trend (profile B), with the aim of stressing more the robustness of regulation. Note that demand profiles A and B share the same average values for each single demand profile. The source pressure head profile is reported in Fig. 4 as well. A leakage percentage of 20% is also considered in this system.

Due to safety reasons, the speed of both PCVs is typically limited. In particular, a maximum speed of 0.01 s⁻¹ is considered for Case Study A, and a maximum speed of 0.0033 s⁻¹ for Case Study B. Note that, in this way, the time required by the two valves to perform a complete closure is the same.

3. Numerical model

This section briefly summarises the approach adopted for the implementation of the WDN simulated environment; for a detailed description of the numerical model adopted for simulations, refer to Galuppini et al. (2019). A Pressure-driven, unsteady flow modelling approach (Ciapponi, Franchioli, Murari, & Papiri, 2015; Creaco, Campisano, Franchini, & Modica, 2017; Streeter, Wylie, & Bedford, 1998) is adopted, in order to allow a proper analysis of the hydraulic transients resulting from rapid nodal demand and/or valve setting variations.

Moreover, to improve the accuracy of the model, pipe friction slopes are increased using the correction proposed by Pezzinga in Pezzinga (2000), to account for the unsteady flow effects. For a generic pipe of a WDN, the one-dimensional unsteady flow equations take the form:

$$\begin{aligned} \frac{\partial h_p}{\partial x} + \frac{1}{gA} \frac{\partial Q_p}{\partial t} + J_p &= 0 \\ \frac{\partial h_p}{\partial t} + \frac{c^2}{gA} \frac{\partial Q_p}{\partial x} + \frac{c^2 q}{gA} &= 0 \end{aligned} \quad (1)$$

where h_p [m] and Q_p [m³/s] are the pressure head and the flow discharge along the pipe, x [m] is the position along the pipe, t [s] is time, A [m²] is the pipe cross-section area, g [m/s²] is the gravity acceleration constant, c [m/s] is the wave celerity, q [m²/s] is the leakage outflow per unit of length, J_p is the friction slope. The wave celerity c can be related to physical quantities of water and of the pipe as follows:

$$c = \left(\frac{\frac{\epsilon}{\zeta}}{1 + \frac{\epsilon d}{E_s}} \right)^{\frac{1}{2}} \quad (2)$$

where ϵ [Pa] and ζ [kg/m³] are water bulk modulus and density; E [Pa], d [m] and s [m] are pipe modulus of elasticity, diameter and thickness.

The presence of leakage from WDN pipes is considered by means of the following outflow q :

$$q = \alpha_{leak} h_p^{\gamma_{leak}} \quad (3)$$

where α_{leak} [m/s] and γ [–] are the leakage coefficient and exponent, respectively. As for leakage evaluation, exponent γ_{leak} is set to 1, typical value for plastic pipes (Van Zyl & Cassa, 2013). Coefficient α_{leak} [–] is set to 0 and $9.4 \cdot 10^{-9}$ m/s to obtain a leakage percentage rate of 0% and 20%, in the two case studies, respectively.

Finally, each pipe friction slope is evaluated as:

$$J_p = 10.29 \frac{n^2 |Q_p| Q_p}{d^{5.33}} \quad (4)$$

where n [s/m^{1/3}] is the Gauckler–Manning coefficient, and then increased using the correction proposed by Pezzinga (2000).

The effect of the control valve is modelled by considering no link at the valve site and setting nodal inflow at the upstream end at:

$$Q_{up} = \sqrt{\frac{2g}{\xi(\alpha)}} A \sqrt{\Delta H_{valve}} \quad (5)$$

The inflow at the downstream end is set, instead, at:

$$Q_{down} = Q_{up} \quad (6)$$

where A [m²] is the valve cross-section area, g [m/s²] is the gravity acceleration constant, ξ is the valve head loss coefficient, ΔH_{valve} is the head drop in the valve and α is the valve closure setting, ranging from 0 (fully open) to 1 (fully closed). The valve head loss coefficient is a growing function of α . This function is typically made available by the valve manufacturer. An example is depicted in Fig. 5.

Some realistic measurement noises $n_h(t)$ and $n_q(t)$ are present, acting respectively on the pressure $h(t)$, and on the flow at the valve site $Q(t)$.

In the model implementation, the water hammer partial differential equations are solved by relying on the method of the characteristics (Streeter et al., 1998).

4. Control algorithm design methodology

This section summarises the key points of the $F^1 PI-SP-gs$ control algorithm originally discussed in Galuppini, Creaco et al. (2020), which can be consulted for further details. The overall control scheme is depicted in Fig. 6. For sake of compactness, in this work, the control algorithm will be referred to simply as $F^1 PI$.

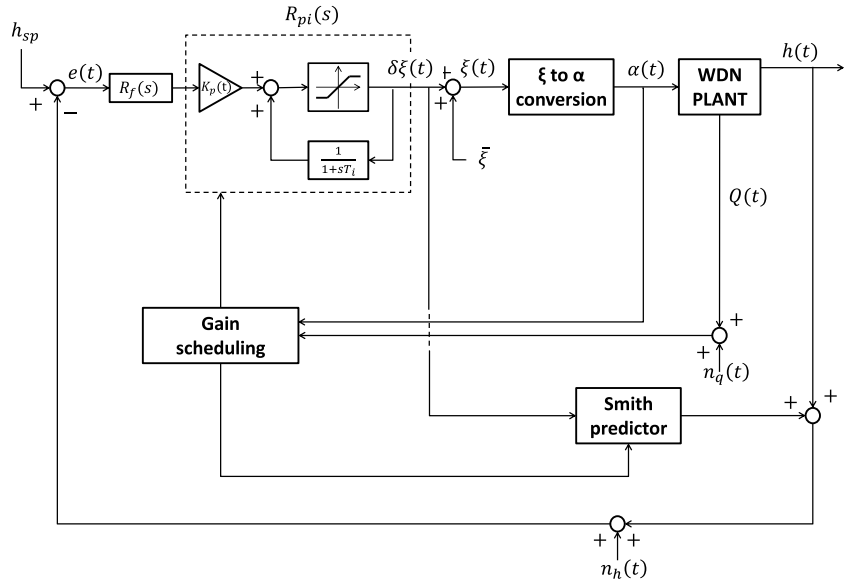


Fig. 6. Complete block scheme for the $F^1 PI - SP - gs$ control algorithm including regulator with antiwindup implementation, Smith predictor and gain scheduling policies.

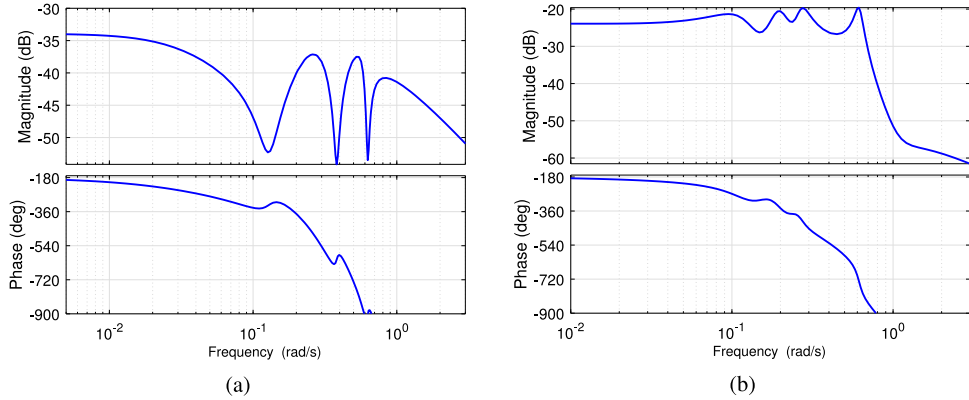


Fig. 7. (a) Bode diagram of the transfer function $G(s)$ for Case Study A (a) and Case Study B (b).

- **Definition of the nominal working point (WP) of the MIMO system.** The input signals are $\xi(t)$, $H(t)$ and $D_i(t)$, i.e. the local head loss coefficient ($[-]$), the source pressure head ($[m]$) and the water demand ($[m^3/s]$) at node i , respectively. The output signals are $h(t)$ and $Q(t)$, i.e. the pressure at the critical node of the WDN ($[m]$) and the flow at the valve site ($[m^3/s]$), respectively. Let $\xi(\alpha(t))$ be control variable, $H(t)$ and $D_i(t)$ be stochastic disturbances acting on the process. Since the average values of typical $H(t)$ and $D_i(t)$ profiles are usually available to the WDN manager, it is possible to consider such value as inputs to the system for the definition of the WP. Under this assumption, it is possible to define of the value of ξ resulting in the desired pressure $h = h_{sp}$ and in a flow at the valve site Q . In this scenario, the tuple $WP_A = (\bar{\xi}, \bar{H}, \bar{D}_1, \bar{h}, \bar{Q})$ represents the working point for Case Study A, and the tuple $WP_B = (\bar{\xi}, \bar{H}, \bar{D}_1, \dots, \bar{D}_{N_{nodes}}, \bar{h}, \bar{Q})$ the working point for Case Study B.

- **Identification of a linear, SISO model describing the system dynamics around WP.**

Provided that the curve $\xi(\alpha)$ is known, a transfer function $G(s)$, describing a SISO system with input signal $\delta\xi(t) = \xi(t) - \bar{\xi}$ and output signal $\delta h(t) = h(t) - \bar{h}$, can be identified from simulated step response experiments performed around WP. Note that the order of $G(s)$ should be high enough to carefully capture the high frequency resonance peaks that characterise the process under control, as suggested in Galuppini, Magni et al. (2020). In

addition, a pure delay is typically present in $G(s)$, due to the finite speed of propagation of waves throughout the pipes of the WDN. Examples of Bode diagrams of $G(s)$ are reported in Figs. 7(a) and 7(b).

- **Nominal control design.**

The nominal control design is based on the transfer function $G(s)$, and aims at regulating the pressure $h(t)$ to the setpoint h_{sp} , in presence of process disturbances generated by the effect of exogenous inputs $H(t)$ and $D_i(t)$. A Smith predictor is introduced to compensate for the effect of the pure delay present in $G(s)$. A manual shaping of the loop function $L(s)$, by acting on the regulator transfer function $R(s)$, was then considered in previous works (Galuppini, Creaco et al., 2020; Galuppini et al., 2019). This paper proposes a new approach for the design of $R(s)$, based on the solution of a bi-objective optimisation problem, as discussed in the following sections.

Note that, due to the presence of a control action saturation (physical valve), if an integrator is present in the regulator transfer function, an antiwindup implementation has to be preferred. As shown in Fig. 6, the Proportional–Integral block is implemented by introducing a model of the saturation (expressed in terms of $\delta\xi$), so that the inner, positive feedback loop results in the desired $R_{pi}(s)$ when the saturation is not active, while integration is limited to the minimum or maximum admissible control action values when the saturation gets active (Magni & Scattolini, 2014).

Finally, all transfer functions involved in the control scheme are discretised by means of *Tustin* method, to preserve their stability properties, with a proper sampling time according to Nyquist sampling theorem (Seborg, Mellichamp, Edgar, & Doyle, 2010).

- *Definition of a nonlinearity inversion block and a gain scheduling policy for the regulator static gain.*

Note that the choice of $\xi(\alpha(t))$ as control variable, opposed to $\alpha(t)$, is motivated by the strong nonlinearity of the $\xi(\alpha(t))$ curve. Due to the time-varying nature of exogenous inputs, the system typically moves far away from its nominal WP. This can result in an increase in the process gain and, eventually, endanger the closed-loop system. To cope with this effect, since the $\xi(\alpha(t))$ curve is typically available and invertible, a nonlinearity inversion block can be introduced in the control loop to compute, at each time instant, the value of α that corresponds to the valve head loss coefficient ξ required by the regulator. Moreover, a gain scheduling policy for $R(s)$ is introduced to compensate for process gain nonlinearities related to the flow Q , thus improving the robustness of the control scheme, and balance between cost of control and regulation error at different working points. Note that the introduction of the gain scheduling does not affect the methodology adopted for the nominal design phase, but may allow to reduce conservatism in terms of robustness margins associated with the design. Further details about gain scheduling can be found in Appendix C and in Galuppini, Creaco et al. (2020).

5. Nominal control design based on bi-objective optimisation

The main goal of this work is to propose a new methodology for the design of the regulator transfer function $R(s)$, based on the solution of a bi-objective optimisation problem that formalises the main specifications for the closed-loop (linearised) system, both in terms of performance and robustness. As discussed earlier in this work, due to the complex shape of the process transfer function $G(s)$, it may be difficult to define a proper target loop function $L^*(s)$ and minimise its distance from the actual loop function $L(s) = R(s)G(s)$. To overcome the problem, it is possible to define an optimisation problem, where robustness specifications are expressed as constraints, and performance specifications are expressed as objective functions, with reference to the loop function $L(s)$. Moreover, to provide a more complete overview of the trade-off arising in the design of the sensitivity function $S(s) = 1/(1+L(s))$ and the complementary sensitivity function $F(s) = L(s)/(1+L(s))$, the optimisation problem is formulated as a bi-objective one. Its solution results in a Pareto front, where each point represents an optimal combination of the two objective functions. The knowledge of the Pareto front should help the designer in selecting the final tuning for $R(s)$, or a set of candidate tunings to be tested on the nonlinear plant. The overall nominal regulator design is discussed in details in the following subsections.

5.1. Design specifications

The main control goal are the regulation of the measured pressure $h(t)$ at the setpoint h_{sp} , and the rejection of process disturbances arising from time varying users' demand and source pressure. This translates in a low magnitude of the sensitivity function $S(s)$ in correspondence to the main harmonic content of the process disturbances. Additionally, the presence of an integrator in the loop function (introduced with $R(s)$), in the absence of derivative actions, guarantees robust regulation of step disturbances, such as those arising from fire hydrant operations (Creaco, Campisano, & Modica, 2018), and perfect tracking of step reference signals. In this respect, to ensure a prompt reaction, the closed-loop bandwidth should be large enough to obtain a closed-loop settling time in the order of tenths of seconds.

Moreover, the closed-loop should attenuate the resonant behaviour characterising the high frequency dynamics of the process under control. As discussed in Galuppini, Magni et al. (2020), this helps improving robustness of the closed-loop and reducing the control effort associated with regulation. This translates in a low magnitude of the complementary sensitivity function $F(s)$ in correspondence to the frequency associated with the main resonance peaks of $G(s)$.

Finally, Galuppini, Magni et al. (2020) also suggests that, in view of the complexity of the system dynamics, different robustness indicators should be adopted to provide the closed-loop design with a proper degree of robustness against different model uncertainties: for this purpose, phase margin ϕ_m , gain margin k_m and vector margin Δ_m are all included in the design of the loop function. Complete definitions of ϕ_m , k_m and Δ_m are reported in Appendix A, while more detailed discussion of the role of each robustness indicator is given in the following of this section.

5.2. Pure delay compensation

As discussed earlier in this work, $G(s)$ is typically characterised by a pure delay. Let $G'(s)$ be the rational part of $G(s)$, i.e. $G(s) = G'(s)e^{-s\tau}$. According to Galuppini et al. (2019), Galuppini, Magni et al. (2020) and Fontana, Giugni, Glielmo, Marini, and Verrilli (2017), Fontana, Giugni, Glielmo, Marini, and Zollo (2017), a Smith predictor is effective in compensating for the effect of the pure delay in the WDN framework. It is then possible to introduce in the control loop a Smith predictor with transfer function $P(s)$ given by:

$$P(s) = (1 - e^{-s\tau})G'(s) \quad (7)$$

and base the loop design on $G'(s)$ only.

5.3. Bi-objective optimisation problem formulation

Consider the process transfer function $G'(s)$. Note that, in this framework, $G'(s)$ is typically asymptotically stable, due to the dissipative nature of the process it describes. Moreover, following to Section 5.2, assume $G'(s)$ does not contain any pure delay term. Let μ_g be its static gain; let also define $\mathcal{W}_{rp} = \{\omega_{rp_1}, \omega_{rp_2}, \dots\}$ as the set of frequencies associated with the resonance peaks of $G'(s)$.

Let now introduce the *F¹PI* regulator structure, whose transfer function is given by:

$$R(s) = R_{pi}(s)R_f(s) \quad (8)$$

with:

$$R_{pi}(s) = \mu_r \frac{1 + sT_i}{s} \quad (9)$$

$$R_f(s) = \frac{(1 + sT_d)}{(1 + sT_f)} \quad (10)$$

Note that $R(s)$ represents the cascade of a Proportional–Integral regulator $R_{pi}(s)$ and a unitary gain filter $R_f(s)$, with order one and zero relative degree. This regulator structure was proven to provide good results in Galuppini et al. (2019), Galuppini, Magni et al. (2020).

Let Θ be the vector of optimisation variables:

$$\Theta = [\mu_r \ T_i \ T_f \ T_d]^\top \quad (11)$$

with $^\top$ denoting the transpose operator. It holds then:

$$L'(s, \Theta) = R(s, \Theta)G'(s) \quad (12)$$

$$S'(s, \Theta) = 1/(1 + L'(s, \Theta)) \quad (13)$$

$$F'(s, \Theta) = L'(s, \Theta)/(1 + L'(s, \Theta)) \quad (14)$$

In addition, let $\mu_L(\Theta) = \mu_r \mu_g$ be the static gain of $L'(s, \Theta)$, and $\omega_c(\Theta)$ its critical frequency, i.e. $|L'(j\omega_c(\Theta))| = 1$. Finally, let $\mathcal{P}_F = \{p_{F_1}, p_{F_2}, \dots\}$ be the set of the poles of $F'(s, \Theta)$.

At this point, two objective functions can be defined as follows:

$$J_1(\Theta) = -|\mu'_L(\Theta)\omega_c(\Theta)| \quad (15)$$

$$J_2(\Theta) = \max_{\omega_{rp} \in \mathcal{W}_{rp}} (|L'(j\omega_{rp}, \Theta)|) \quad (16)$$

For sake of simplicity, let now refer to $-J_1$ also as *Gain-Bandwidth Product* (GBP) and to J_2 also as *Maximum Peak Height* (MPH).

The bi-objective optimisation problem is then given by:

$$\min_{\Theta} (J_1(\Theta), J_2(\Theta)) \quad (17)$$

subject to :

$$\operatorname{Re}\{p_F\} < 0 \quad \forall p_F \in \mathcal{P}_F \quad (18)$$

$$\phi_m(\Theta) \geq \underline{\phi}_m \quad (19)$$

$$k_m(\Theta) \geq \underline{k}_m \quad (20)$$

$$\Delta_m(\Theta) \geq \underline{\Delta}_m \quad (21)$$

$$\max_{\omega_{rp} \in \mathcal{W}_{rp}} (|L(j\omega_{rp}, \Theta)|) \leq \bar{L}_{rp} \quad (22)$$

$$T_i, T_f, T_d > 0 \quad (23)$$

$$\mu_r \mu_g > 0 \quad (24)$$

with $\underline{\phi}_m > 0$, $\underline{k}_m > 1$, $\underline{\Delta}_m > 0$, $\bar{L}_{rp} < 1$.

In the following of this work, let refer to the bi-objective optimisation problem (17)–(24) as *Regulator Tuning Bi-Objective Optimisation Problem* (RT-BOOP).

The minimisation of $J_1(\Theta)$ requires the critical frequency of $L'(s)$ to be the largest possible and, at the same time, its static gain to be the largest possible. Due to the presence of an integrator in $L'(s)$, this forces the whole $|S'(j\omega)|$ to be the small for $\omega < \omega_c$, while forcing ω_c to be the largest possible. On the other hand, the minimisation of $J_2(\Theta)$ requires the magnitude of $F'(s)$ to be the lowest possible in correspondence of its highest resonance peak, which acts as upper bound and forces all resonance peaks of $F'(s)$ to be deamplified. Moreover, this also helps reducing the magnitude of the control sensitivity function $Q'(s) = R(s)S'(s)$ at high frequency, possibly reducing the control effort (Galuppini, Magni et al., 2020). The combined minimisation of both objective functions expresses then the typical trade-off that arises in the design of the loop functions $S'(s)$ and $F'(s)$, since, by definition, it holds $F'(s) + S'(s) = 1$ (Magni & Scattolini, 2014). Note that the choice of $J_1(\Theta)$ as the product of μ_L and ω_c ensures that they are both maximised. In fact, the presence of μ_L alone in the objective function may result in ω_c assuming arbitrarily low values, thus spoiling the design trade-off. On the contrary, the presence of ω_c alone may result in arbitrarily low values of μ_L and not guarantee enough disturbance rejection at low frequency. In both cases, problems may arise due to low frequency singularities of $L'(s)$, whose presence is therefore not favoured by the choice of the objective functions.

As far as constraints are concerned, (18) forces closed-loop stability; constraint (19) requires a minimum phase margin ϕ_m , to account for uncertainties affecting the estimation of the pure delay τ and the position of poles and zeros of $G'(s)$, which may also depend on the operating point. Moreover, it also allows to control the amount of overshoot and oscillations in the closed-loop step response (Magni & Scattolini, 2014). Constraint (20) requires a minimum gain margin k_m , to account for gain uncertainties and uncertainties in the $\xi(\alpha)$ characteristic curve of the valve, which is exploited for nonlinearity compensation (Galuppini, Creaco et al., 2020); finally, in view of the complex shape of the loop function, constraint (21) is particularly useful to provide minimum robustness level at each frequency, as stressed in Galuppini, Magni et al. (2020). Constraint (22) can be interpreted both as a robustness requirement (the presence of poorly deamplified resonance peaks of $L'(s)$ may result in closed-loop instability (Galuppini, Magni et al., 2020), and as a minimum performance requirement for $J_2(\Theta)$. Finally, constraints (23)–(24) place bounds on the optimisation variables. In

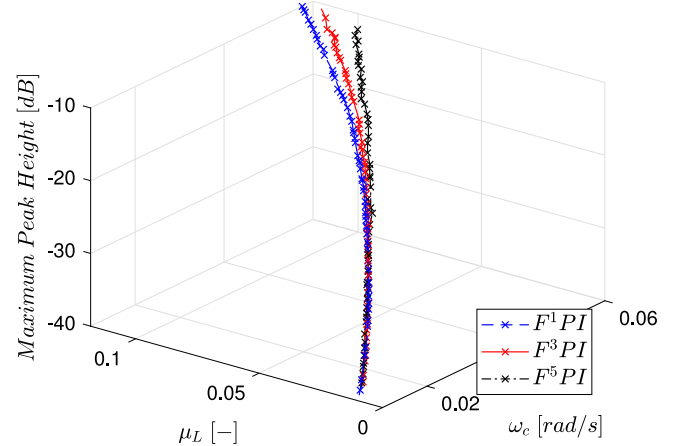


Fig. 8. Case Study A. 3D Pareto fronts resulting from the solution of the RT-BOOP.

particular, all singularities of $R(s)$ are required to lie in the left-hand side of the real axis, to avoid unstable poles or non-minimum phase zeros, and the static gain of the regulator is required to share its sign with the gain of $G'(s)$.

Note that the solution of RT-BOOP is given by a Pareto-optimal set, i.e. a set of non-dominated, feasible solutions. A feasible solution $\Theta^{(1)}$ is said to dominate a feasible solution $\Theta^{(2)}$ if both the following conditions hold (Deb, 2001):

- $J_i(\Theta^{(1)}) \leq J_i(\Theta^{(2)})$, $\forall i \in \{1, 2\}$;
- $\exists i^* \in \{1, 2\}$ s.t. $J_{i^*}(\Theta^{(1)}) < J_{i^*}(\Theta^{(2)})$.

The image of the Pareto-optimal set through $J_1(\Theta)$ and $J_2(\Theta)$ defines the associated Pareto-optimal front.

5.4. Tuning performances selection

As discussed in the previous Section, the solution of RT-BOOP provides the decision maker with a set of possible regulator tunings (the Pareto set), along with three metrics (static gain, critical frequency and peak attenuation) related to the linear system framework. At this point, the designer has to select the desired tuning among the possible solutions, according to both expected performances and, possibly, further considerations regarding the process under control. For this purpose, it may be profitable to move to a three dimensional representation of the front, as depicted in Fig. 8, and consider the three features of the loop function in a pairwise way, as in Fig. 9, by considering the projections of the 3D front on the (μ_L, ω_c) plane, (MPH, ω_c) plane and (MPH, μ_L) plane. The analysis of each feature allows to obtain different information about the expected closed-loop performances: the static gain provides information about disturbance rejection, especially at low frequency, while the critical frequency provides information about both disturbance rejection, placing an upper bound to the maximum disturbance frequency that can be rejected, and closed-loop settling time. The peak attenuation factor provides information about the high frequency behaviour of the closed-loop system. Further information about the process, such as the power spectral density of disturbances, a requirement on the settling time, or a constraint on sampling time, can guide the designer in the choice of the final tuning to be tested on the nonlinear plant.

For instance, information about users' demand main frequency components, which represent the main source of disturbance acting on the plant, can be obtained by monitoring a significant subset of users (Fiorillo, Galuppini et al., 2020), or adopting a proper mathematical modelling (Fiorillo, Creaco, De Paola, & Giugni, 2020). It is then straightforward to compute, for each tuning, the disturbance rejection factor at each frequency of interest ω_d , as $|S(j\omega_d)|$.

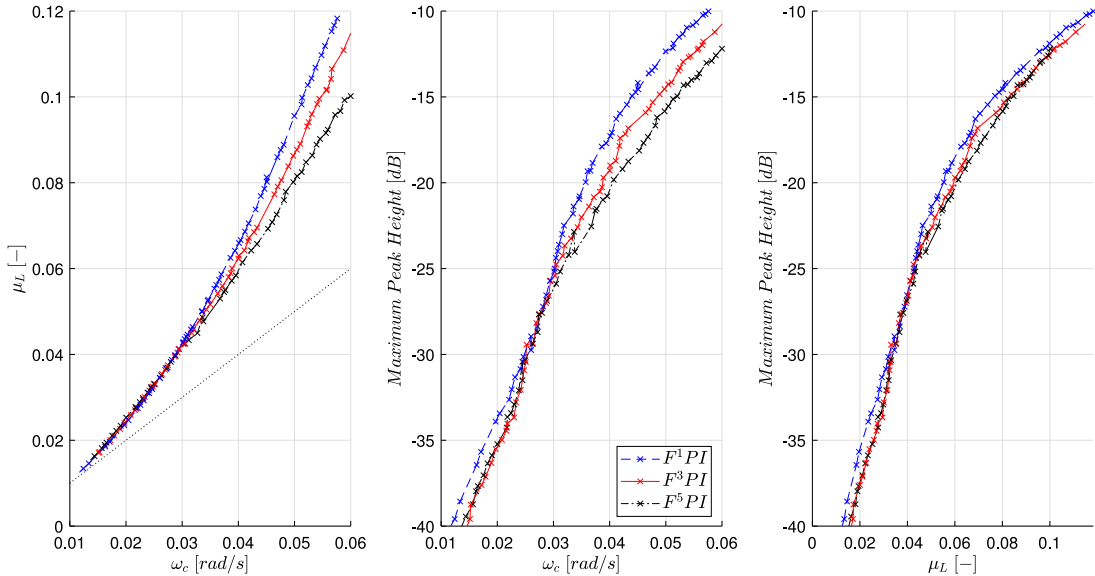


Fig. 9. Case Study A. Projections of 3D Pareto fronts resulting from the solution of the RT-BOOP in the (μ_L, ω_c) plane, (MPH, ω_c) plane and (MPH, μ_L) plane for different regulator structures. The bisector line of the (μ_L, ω_c) plane is also depicted (grey, dotted line).

In presence of a requirement on the maximum closed-loop settling time, or on its order of magnitude, it is also possible to compute, for each tuning, the expected 95% settling time for the linear, second order approximation of the closed-loop as:

$$T_{0.95} = \frac{4.6}{0.01\phi_m\omega_c} + \tau. \quad (25)$$

with τ the pure delay affecting $G(s)$ (Seborg et al., 2010), and choose accordingly.

Moreover, the sampling time of the signals involved in the control loop may pose further constraints on the choice of the tunings, in particular on the critical frequency: let T_s be the minimum sampling time available, expressed in seconds. The corresponding maximum Nyquist frequency $\overline{\omega_N}$ is given by:

$$\overline{\omega_N} = \frac{\pi}{T_s} \quad (26)$$

and the critical frequency must therefore fulfil:

$$\omega_c < \gamma \overline{\omega_N} \quad (27)$$

with $0 < \gamma < 1$ (typically $\gamma < 0.2$) (Seborg et al., 2010). A possibility is selecting a tuning that fulfils this additional constraint and provides sufficient attenuation of signals from the Nyquist frequency and above: this is can be done by considering J_2 . Finally, the choice of the tuning should also take into account the phase margin loss due to discretisation of $R(s)$ (Seborg et al., 2010), which is given by:

$$\phi_{Ts} = -\frac{T_s}{2} \omega_c \frac{180}{\pi} \quad (28)$$

5.5. Bi-objective optimisation problem solution with Genetic Algorithm

For this work, RT-BOOP is solved by means of Matlab Multi-Objective Genetic Algorithm, based on NSGA-II Genetic Algorithm (Deb, Pratap, Agarwal, & Meyarivan, 2002). To speed up computations, the parallel implementation is preferred, while constraints of RT-BOOP are implemented as *soft constraints*, with a *static penalty function*, as suggested in Deb (2001). Note that, while the penalty constant for constraint violation impacts on the distortion of the objective functions, genetic algorithms provide low sensitivity to such distortions (Deb, 2001). Furthermore, suitable upper and lower bounds can be placed on optimisation variables to reduce the size of the search space.

Note that the solution of RT-BOOP obtained with NSGA-II Genetic Algorithm is a finite dimension set of feasible solutions, where each solution belonging to the set is not dominated by any other solution in the set. This set approximates the Pareto-optimal set, and its image through the objective functions $J_1(\Theta)$ and $J_2(\Theta)$ approximates the Pareto-optimal front (Deb, 2001). Let this set be denoted as Θ^{PF} .

It must be remarked that the final set of solutions Θ^{PF} depends on the initialisation of the population of NSGA-II. To overcome this problem, and improve the stability of the Pareto fronts, it is possible to obtain a number of preliminary solutions to RT-BOOP and construct a population from such solutions to be used as initial population for a final run of NSGA-II.

For sake of simplicity, the set of solutions provided by NSGA-II and its image through the objective functions will be referred to simply as *Pareto front* in the following of this work.

5.5.1. Regulator tuning computation

This subsection briefly discusses the computation of the regulator tuning, denoted as Θ^* , that results in the desired performances, starting from the set of solutions obtained solving RT-BOOP with NSGA-II. If the front is sufficiently crowded (i.e. the solutions defining the front are not too distant from each other), a simple linear interpolation can be used to invert one of the three curves $\mu_L(\Theta)$, $\omega_c(\Theta)$, or $MPH(\Theta)$ with $\Theta \in \Theta^{PF}$, and obtain Θ^* starting from the desired value. For instance, assume to fix a feasible value for ω_c , and let it be denoted as ω_c^* . It is then possible to find two solutions $\Theta_u \leq \Theta_l \in \Theta^{PF}$ such that the corresponding values $\omega_c(\Theta_u)$ and $\omega_c(\Theta_l)$ are the those that better approximate ω_c^* from above and from below, respectively, and apply linear interpolation to compute Θ^* such that $\omega_c(\Theta^*) = \omega_c^*$. An *a posteriori* check of the resulting tuning is then advisable, to verify constraint satisfaction and consistency of the objective functions with the desired values.

In case the above approach is not viable or results in poorly reliable results, it is possible to fix J_1 or J_2 and solve the mono-objective version of the bi-objective problem (17)–(24), where one of the two objective functions is replaced by a constraint. For instance, assume to fix a feasible value for J_2 , and let it be denoted as J_2^* . Then:

$$\Theta^* = \arg \min_{\Theta} J_1(\Theta) \quad (29)$$

$$\text{subject to :} \quad (30)$$

$$J_2(\Theta) = J_2^* \quad (31)$$

plus constraints (18)–(24).

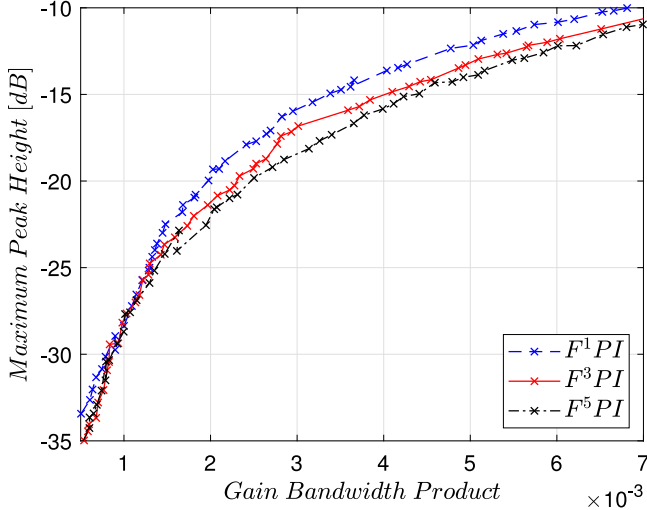


Fig. 10. Case Study A. Pareto fronts resulting from the solution of the RT-BOOP.

5.6. Extension to $F^n PI$ regulator structures

The tuning approach presented in this section formulates the typical trade-off in the design of sensitivity and complementary functions as a bi-objective optimisation problem, to explicitly account for different design goals. In particular, the approach was presented with reference to a particular regulator structure, defined as $F^1 PI$. The extension to more complex regulator structures is straightforward. For instance, it may be useful to increase the number of poles and zeros of $R_f(s)$ to allow more degrees of freedom in the design of $L'(s)$. Let then define the more general $F^n PI$ as follows:

$$R(s) = R_{pi}(s)R_f(s) \quad (32)$$

with:

$$R_f(s) = \frac{\prod_{i=1}^n (1 + sT_{d_i})}{\prod_{i=1}^n (1 + sT_{f_i})} \quad (33)$$

The vector of optimisation variables can be extended as:

$$\Theta = [\mu_r \ T_i \ T_{f_1} \ \dots \ T_{f_n} \ T_{d_1} \ \dots \ T_{d_n}]^\top \quad (34)$$

and constraint (23) replaced by:

$$T_i, T_{f_1}, \dots, T_{f_n}, T_{d_1}, \dots, T_{d_n} > 0 \quad (35)$$

Remark: A comparison of the Pareto fronts related to different regulator structures may highlight possible improvements in both objective functions thanks to more complex regulators (an example from Case Study A is reported in Fig. 10). Still, it must be remarked that, since the design of regulators is based on a linear, local approximation of the system dynamics, it may be profitable to select a set of candidate tunings to be tested on the nonlinear plant, and directly evaluate their performances with experiments on the nonlinear plant. On the other hand, the robustness margins provided by the nominal tunings, along with the nonlinearity compensation strategies described in Galuppini, Creaco et al. (2020), allow performing experiments with very little risk of instability of the overall closed-loop system; finally a more complex regulator transfer function only introduces a negligible overhead in terms of computational effort.

6. Regulator tuning results

6.1. Case study A

As described in Section 4, the design of the control algorithms starts with the identification of the WP of the system, and the identification of

Table 1

Case Study A. Features of the loop functions obtained with $\omega_c^* = 0.05$ rad/s and $F^1 PI$, $F^1 PI$ manual and $F^5 PI$ algorithms.

	$F^1 PI$	$F^1 PI$ manual	$F^5 PI$
ϕ_m [°]	45	48	45
k_m [-]	∞	∞	∞
Δ_m [-]	0.680	0.670	0.640
μ_L [-]	0.096	0.050	0.080
ω_c [rad/s]	0.050	0.048	0.050
MPH [dB]	-12	-12	-15

a SISO transfer function $G(s)$ that approximates the system dynamic in a neighbourhood of WP. In particular, let the WP_A be the working point for Case Study A; its complete definition is reported in Appendix B. Then, the identification phase results in $G_a(s)$, whose Bode diagram is depicted in Fig. 7(a). Moreover, a Smith predictor is introduced in the design, based on $G_a(s)$. Finally, Pareto fronts are obtained by solving RT-BOOP, according to the following specifications:

$$\underline{\phi}_m = 45^\circ \quad \underline{k}_m = 15 \quad \underline{\Delta}_m = 0.5 \quad \overline{L}_{rp} = -10 \text{ dB} \quad (36)$$

with three different filter orders (1, 3 and 5). Projections of 3D Pareto fronts resulting from the solution of the RT-BOOP are depicted in Fig. 9. Note that the values assumed by μ_L and ω_c are almost coincident up to $\omega_c \approx 0.01$ rad/s. This suggests that tunings should result in integrator shaped loop functions, at low frequency, since the presence of low frequency singularities in the loop function $L(s)$ is not favoured in any way in RT-BOOP. At higher critical frequencies, the effect of the filtering component is more evident, and an increase in μ_L does not result in an equal increase in ω_c . To ease this analysis, the bisector of the (μ_L, ω_c) plane is depicted in Fig. 9.

As far as different filter orders are concerned, it is possible to note that higher filter orders dominate lower ones.

For sake of comparison with a manual tuning, loop functions characterised by $\omega_c^* = 0.05$ rad/s are selected. In this case, candidate tunings with filter orders of 1 or 5 are chosen. The regulator parameters are retrieved according to the interpolation procedure described in Section 5.5.1. The resulting loop functions are depicted in Fig. 11(a), along with a manual tuning one from Galuppini, Creaco et al. (2020). Their main features are reported in Table 1.

Note that the actual critical frequency in the case of the manual tuning is slightly lower than the expected one. In addition, the comparison of the manual $F^1 PI$ tuning and the optimisation-based one highlights that the resulting loop functions share a similar magnitude, with the optimisation-based one providing slightly more pronounced deamplification of the first resonance peak, and the manual one providing instead more deamplification from $\omega \approx 0.4$ rad/s. These differences are more evident in the phase of the two loop functions, and are due to the lowest frequency zero of $R_f(s)$, which is placed at a slightly lower frequency in the case of automatic tuning. Note that the phase margin is not affected by this difference. As far as $F^5 PI$ is concerned, it is possible to note that it allows to obtaining a lower magnitude of the loop function at high frequency, but is in turn characterised by a slightly lower gain at low frequency. This is due to the fact that the phase margin limit is reached by both $F^1 PI$ and $F^5 PI$ tunings, and, once the critical frequency is fixed, further peak deamplification cannot be obtained by placing filtering poles at lower frequency, but only by lowering the gain. The resulting regulator transfer functions are discretised with Tustin method and a sampling time of 1 s, which only introduces a negligible phase margin loss.

A second set of tunings is selected around the knee of the Pareto front, by requiring $\omega_c^* = 0.01$ rad/s. Note that, in this case, $F^1 PI$ and $F^3 PI$ tunings are adopted, since the latter is expected to provide similar performances to those of $F^5 PI$. The resulting loop functions are depicted in Fig. 11(b), and their main features summarised in Table 2.

Both loop functions correctly reproduce an integrator at low frequency, while the filtering action starts to appear after the critical

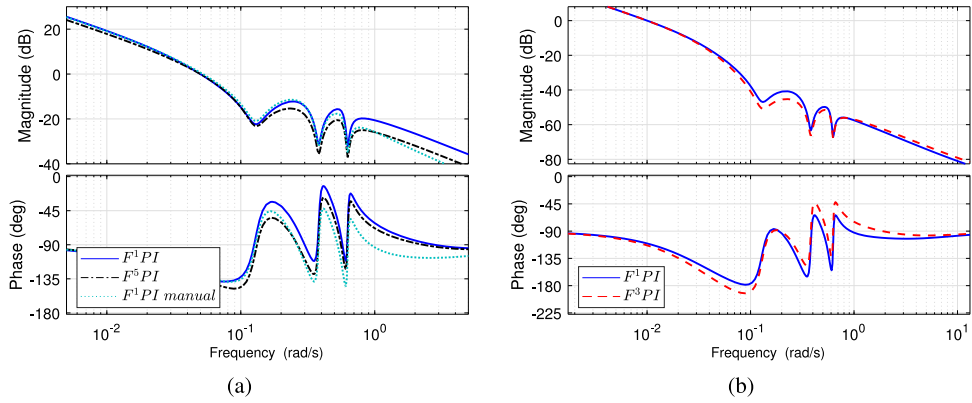


Fig. 11. Case Study A. (a) Bode diagram of the transfer function $L(s)$ obtained with $F^1 \text{PI}$ (blue, solid line), $F^5 \text{PI}$ (black, dashed-dotted line) and, $F^1 \text{PI}$ with manual tuning (cyan, dotted line). The three functions are characterised by $\omega_c^* = 0.05 \text{ rad/s}$. (b) Bode diagram of the transfer function $L(s)$ obtained with $F^1 \text{PI}$ (blue, solid line), $F^3 \text{PI}$ (red, dashed line). The two functions are characterised by $\omega_c^* = 0.01 \text{ rad/s}$.

Table 2
Case Study A. Features of the loop functions obtained with $\omega_c^* = 0.01 \text{ rad/s}$ and $F^1 \text{PI}$ and $F^3 \text{PI}$ algorithms.

	$F^1 \text{PI}$	$F^3 \text{PI}$
$\phi_m [^\circ]$	70	66
$k_m [-]$	∞	15
$\Delta_m [-]$	0.080	0.760
$\mu_L [-]$	0.010	0.010
$\omega_c [\text{rad/s}]$	0.010	0.010
$MPH [\text{dB}]$	-41	-45

Table 3
Case Study B. Features of the loop functions obtained with $\omega_c^* = 0.03 \text{ rad/s}$ and $F^1 \text{PI}$, $F^1 \text{PI}$ manual and $F^3 \text{PI}$ algorithms.

	$F^1 \text{PI}$	$F^1 \text{PI}$ manual	$F^3 \text{PI}$
$\phi_m [^\circ]$	71	70	64
$k_m [-]$	33	19	45
$\Delta_m [-]$	0.820	0.770	0.770
$\mu_L [-]$	0.033	0.030	0.034
$\omega_c [\text{rad/s}]$	0.030	0.026	0.030
$MPH [\text{dB}]$	-12	-15	-15

frequency. Moreover, both loop function provide a strong attenuation of resonance peaks, with 40 dB for $F^1 \text{PI}$ algorithm and 45 dB for $F^3 \text{PI}$. The enhanced high frequency rejection ability comes at the price of a strongly reduced gain margin, while the phase margin is just reduced by few degrees. Still, a closer look at the phase diagram of the loop functions underlines that, in case of phase uncertainty, the phase margin provided by $F^1 \text{PI}$ may be strongly overestimated, since the phase of the loop function almost reaches -180° in correspondence of $\omega \approx 0.1 \text{ rad/s}$. In this scenario, the phase margin provided by $F^3 \text{PI}$ would be wider than that provided by $F^1 \text{PI}$. As in the previous case, regulator transfer functions are discretised with Tustin method and a sampling time of 1 s.

6.2. Case study B

Let now focus on the analysis of the Pareto fronts and on the results of simulations obtained for Case Study B. For a complete definition of the working point, WP_B , see Appendix B. The Bode diagram of $G_b(s)$ is depicted in Fig. 7(b). As for case Study A, a Smith predictor is introduced to compensate for the effect of pure delay, and RT-BOOP solved according to the following specifications:

$$\phi_m = 60^\circ \quad k_m = 30 \quad \Delta_m = 0.7 \quad \bar{L}_{rp} = -10 \text{ dB} \quad (37)$$

Projections of 3D Pareto fronts resulting from the solution of RT-BOOP are depicted in Fig. 12. Filter orders 1, 3 and 5 are considered.

Table 4
Case Study B. Features of the loop functions obtained with $\omega_c^* = 0.01 \text{ rad/s}$ and $F^1 \text{PI}$ and $F^3 \text{PI}$ algorithms.

	$F^1 \text{PI}$	$F^3 \text{PI}$
$\phi_m [^\circ]$	83	78
$k_m [-]$	89	198
$\Delta_m [-]$	0.940	0.880
$\mu_L [-]$	0.010	0.010
$\omega_c [\text{rad/s}]$	0.010	0.010
$MPH [\text{dB}]$	-22	-27

The analysis highlights that μ_L and ω_c are almost coincident up to $\omega_c \approx 0.02 \text{ rad/s}$, resulting in an integrator shaped loop function at low frequency. At higher critical frequencies, the effect of the filtering component is more evident, and an increase in μ_L does not result in an equal increase in ω_c . Moreover, when comparing different filter orders, it is possible to note that $F^3 \text{PI}$ always dominates $F^1 \text{PI}$, but is not dominated by $F^5 \text{PI}$. Candidate tunings will then have filter orders of 1 or 3. In particular, for sake of comparison with a manual tuning, loop functions characterised by $\omega_c^* = 0.03 \text{ rad/s}$ are selected. The regulator parameters are retrieved according to the interpolation procedure described in Section 5.5.1. The resulting loop functions are depicted in Fig. 13(a), along with a manual tuning one from Galuppini, Creaco et al. (2020). Their main features are reported in Table 3.

As for Case Study A, the actual critical frequency in the case of the manual tuning is slightly lower than the expected one. In addition, the comparison of the manual $F^1 \text{PI}$ tuning and the optimisation based one highlights that the resulting loop functions are almost identical, with a slightly lower gain in the case of manual tuning. Only slight differences are also present in the phase of the two loop functions. The $F^3 \text{PI}$ tuning manages to produce a loop function whose magnitude is reduced, starting from $\omega \approx 0.1 \text{ rad/s}$, which is close to the frequency of the highest resonance peak. This is obtained by introducing a phase loss, as depicted in the phase diagram. This is also reflected in the phase margin of the two loop functions; also note that, while the gain margin represents the bottleneck for $F^1 \text{PI}$, the phase margin is the bottleneck for $F^3 \text{PI}$. All regulator transfer functions are finally discretised with Tustin method and a sampling time of 1 s. The associated phase margin loss is negligible.

A second set of tunings is selected around the knee of the Pareto front, by requiring $\omega_c^* = 0.01 \text{ rad/s}$. The resulting loop functions are depicted in Fig. 13(b), and their main features summarised in Table 4.

Note that, for both loop functions, $\omega_c = \mu_L$, and an integrator shaped function is obtained up to the critical frequency. Both tunings provide wide robustness margins and strong deamplification of resonance peaks. As for Case Study A, note that the gain margin provided by $F^3 \text{PI}$ may be overestimated since the phase of the corresponding

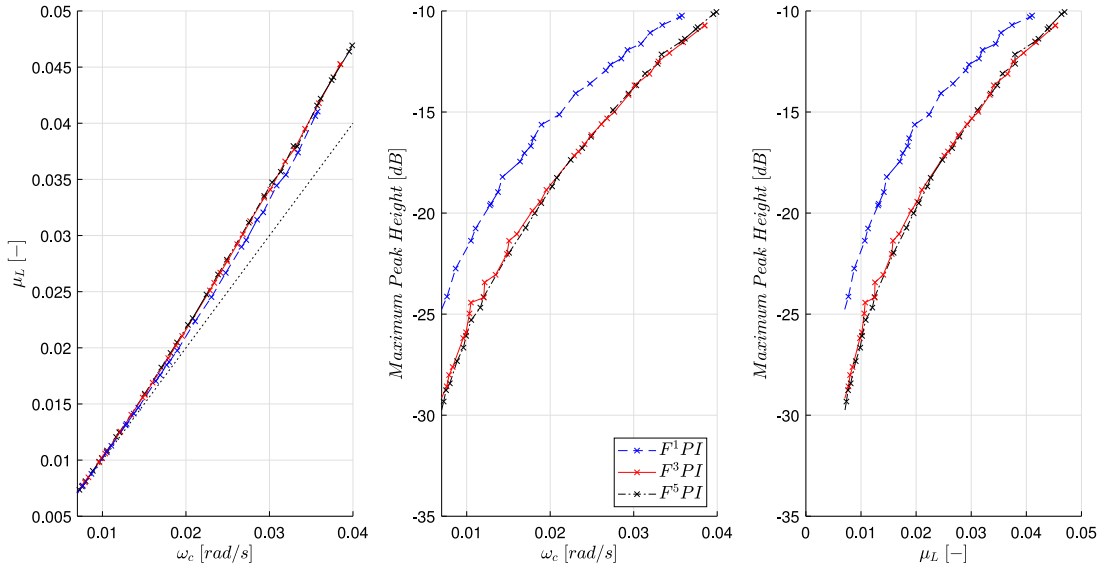


Fig. 12. Case Study B. Projections of 3D Pareto fronts resulting from the solution of the RT-BOOP in the (μ_L, ω_c) plane, (MPH, ω_c) plane and (MPH, μ_L) plane for different regulator structures. The bisector line of the (μ_L, ω_c) plane is also depicted (grey, dotted line).

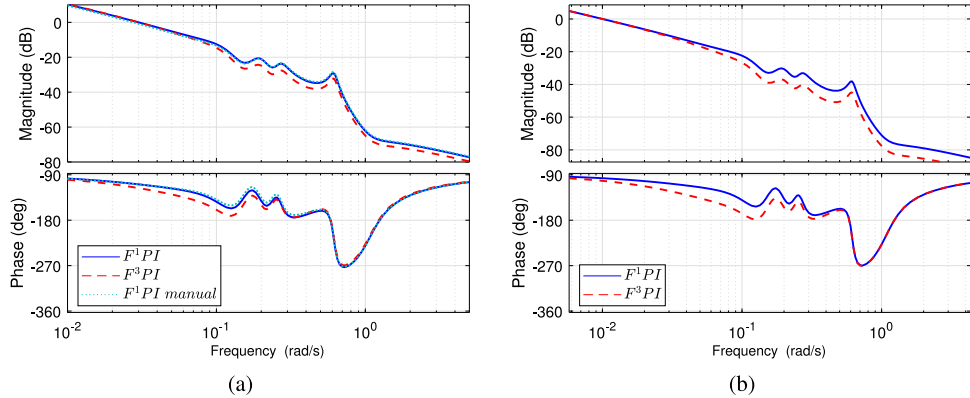


Fig. 13. Case Study B. (a) Bode diagram of the transfer function $L(s)$ obtained with $F^1 PI$ (blue, solid line), $F^3 PI$ (red, dashed line) and, $F^1 PI$ with manual tuning (cyan, dotted line). The three functions are characterised by $\omega_c^* = 0.03$ rad/s. (b) Bode diagram of the transfer function $L(s)$ obtained with $F^1 PI$ (blue, solid line), $F^3 PI$ (red, dashed line). The two functions are characterised by $\omega_c^* = 0.01$ rad/s.

loop function almost reaches a phase of -180° at $\omega \approx 0.1$ rad/s, and can reach it in case of phase uncertainties. Still, the comparison of the function magnitude suggests that, in that case, the gain margin may not be very different from the computed one, which is obtained in correspondence to a resonance peak. Again, regulator transfer functions are finally discretised with Tustin method and a sampling time of 1 s.

7. Simulation results

The different tunings obtained and discussed in the previous section are now applied to the simulated WDNs, to evaluate their effectiveness on the nonlinear, simulated plants. As far as gain scheduling is concerned, the same policy is applied for each comparison, to focus on the effect of the nominal tuning only. Further details about the gain scheduling policy can be found in Galuppini, Creaco et al. (2020).

The results of simulations are evaluated according to the following metrics:

- $Mean|e(k)|$ [m]. The *regulation error*, which evaluates the proximity of the pressure to the desired setpoint.
- $\sum |\Delta\alpha(k)|$ [–]. The *cost of control*, which impacts on the energy required to perform regulation and on wear of actuators.

Table 5

Case Study A. Regulation error for tunings characterised by $\omega_c^* = 0.05$ rad/s.

Demand offset [m^3/s]	$F^1 PI$	$F^1 PI$ manual	$F^5 PI$
-0.03	0.83	0.81	0.84
0	0.56	0.56	0.58
0.05	0.49	0.51	0.49

where $h(k)$ is the measured pressure, h_{sp} is the pressure setpoint, $\alpha(k)$ is the valve closure and $\Delta\alpha(k) = \alpha(k) - \alpha(k-1)$ is the variation of the valve closure over a single sampling time. Let $e(k) = h(k) - h_{sp}$ be the error of the controlled pressure head at time instant k . All signals are sampled with sampling time of 1 s. It should be also remarked that manual tunings from previous works were further refined with trials on the simulated nonlinear plants.

7.1. Case study A

Results of simulations with $F^1 PI$, $F^1 PI$ manual, $F^5 PI$ algorithms, and $\omega_c^* = 0.05$ rad/s are reported in Tables 5 and 6. Fig. 14 depicts the main signals for the simulation with $F^1 PI$. Note that $F^1 PI$ and $F^1 PI$ manual, that share a similar tuning, also produce very similar

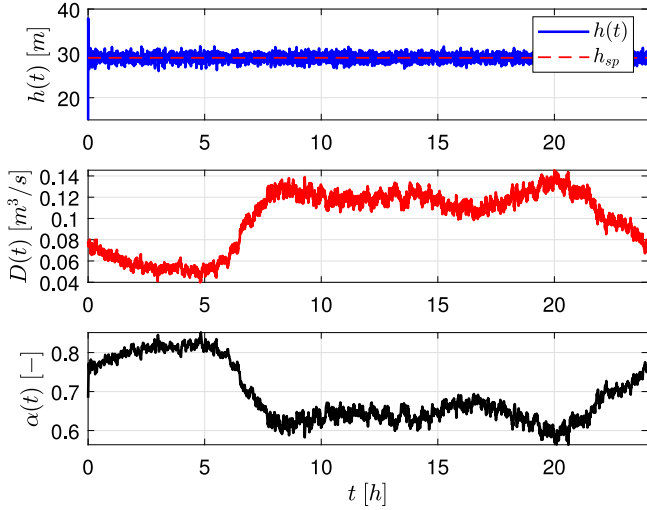


Fig. 14. Case Study A. Closed-loop simulation with $F^1 PI$, $\omega_c^* = 0.05 \text{ rad/s}$, and no demand offset. Top: pressure $h(t)$ and pressure setpoint h_{sp} . Middle: demand $D(t)$. Bottom: valve closure $\alpha(t)$.

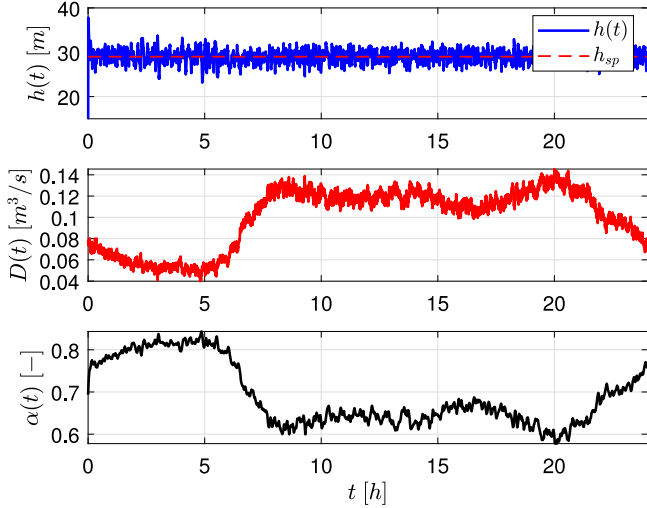


Fig. 15. Case Study A. Closed-loop simulation with $F^1 PI$, $\omega_c^* = 0.01 \text{ rad/s}$, and no demand offset. Top: pressure $h(t)$ and pressure setpoint h_{sp} . Middle: demand $D(t)$. Bottom: valve closure $\alpha(t)$.

Table 6
Case Study A. Cost of control for tunings characterised by $\omega_c^* = 0.05 \text{ rad/s}$.

Demand offset [m^3/s]	$F^1 PI$	$F^1 PI$ manual	$F^5 PI$
-0.03	16.15	15.50	14.54
0	19.89	19.50	18.21
0.05	28.20	28.20	26.80

results, both in terms of regulation error and cost of control; in particular, the manual tuning seems to deliver slightly better performances at low demand operations (demand offset $-0.03 \text{ m}^3/\text{s}$), while the optimisation based one seems to deliver slightly better performances at high demand operations (demand offset $0.05 \text{ m}^3/\text{s}$). On the other hand, $F^5 PI$ consistently improve the cost of control at all demand offsets, at the price of a slightly higher regulation error. Note that this effect may be partially due to the slightly lower gain of the $F^5 PI$ regulator with respect to the other two.

Let now focus on simulations with $F^1 PI$ and $F^3 PI$ algorithms, and $\omega_c^* = 0.01 \text{ rad/s}$. Fig. 15 depicts the main signals for the simulation

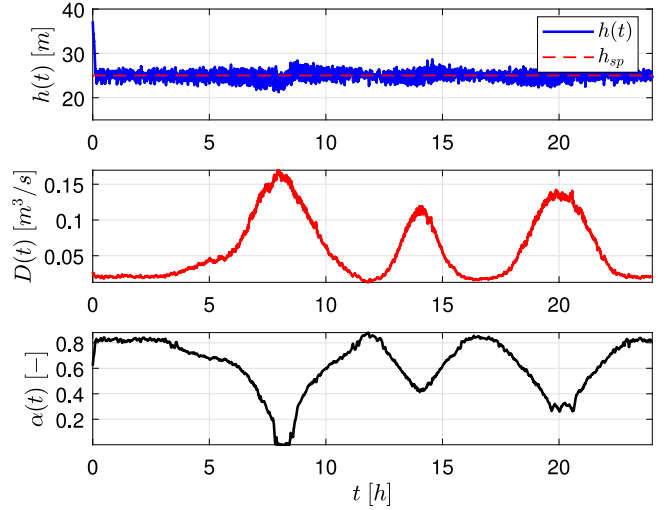


Fig. 16. Case Study B. Closed-loop simulation with $F^1 PI$, $\omega_c^* = 0.03 \text{ rad/s}$, and demand profile B. Top: pressure $h(t)$ and pressure setpoint h_{sp} . Middle: demand $D(t)$. Bottom: valve closure $\alpha(t)$.

Table 7

Case Study A. Regulation error for tunings characterised by $\omega_c^* = 0.01 \text{ rad/s}$.

Demand offset [m^3/s]	$F^1 PI$	$F^3 PI$
-0.03	1.64	1.69
0	1.05	1.08
0.05	0.75	0.76

Table 8

Case Study A. Cost of control for tunings characterised by $\omega_c^* = 0.01 \text{ rad/s}$.

Demand offset [m^3/s]	$F^1 PI$	$F^3 PI$
-0.03	4.99	5.12
0	5.08	5.18
0.05	7.24	7.21

Table 9

Case Study B. Regulation error for tunings characterised by $\omega_c^* = 0.03 \text{ rad/s}$.

Demand profile	$F^1 PI$	$F^1 PI$ manual	$F^3 PI$
A	0.74	0.76	0.77
B	0.67	0.67	0.67

Table 10

Case Study B. Cost of control for tunings characterised by $\omega_c^* = 0.03 \text{ rad/s}$.

Demand profile	$F^1 PI$	$F^1 PI$ manual	$F^3 PI$
A	10.30	9.90	8.90
B	10.28	9.20	9.85

with $F^1 PI$. Metrics are reported in Tables 7 and 8. In this situation, despite the improvement expected from the design in the linear systems framework, $F^3 PI$ does not allow to improve the results. This may be due to the fact that the further high frequency rejection provided by the higher filter order is not useful, since the rejection provided by $F^1 PI$ (41 dB) is sufficient to make the presence of resonance peaks negligible.

7.2. Case study B

Results of simulations with $F^1 PI$, $F^1 PI$ manual, $F^3 PI$ algorithms, and $\omega_c^* = 0.03 \text{ rad/s}$ are reported in Tables 9 and 10. Fig. 16 depicts the main signals for the simulation with $F^1 PI$. The comparison of

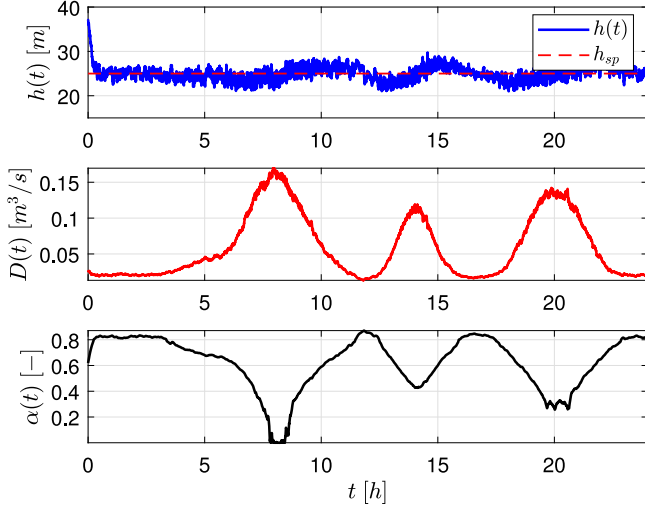


Fig. 17. Case Study B. Closed-loop simulation with $F^1 PI$, $\omega_c^* = 0.01 \text{ rad/s}$, and demand profile B. Top: pressure $h(t)$ and pressure setpoint h_{sp} . Middle: demand $D(t)$. Bottom: valve closure $\alpha(t)$.

Table 11

Case Study B. Regulation error for tunings characterised by $\omega_c^* = 0.01 \text{ rad/s}$.

Demand profile	$F^1 PI$	$F^3 PI$
A	0.92	0.94
B	1.19	1.15

Table 12

Case Study B. Cost of control for tunings characterised by $\omega_c^* = 0.01 \text{ rad/s}$.

Demand profile	$F^1 PI$	$F^3 PI$
A	2.22	2.20
B	5.68	5.19

results obtained with manual and optimisation based $F^1 PI$ algorithms highlights that the regulation error is almost identical, or slightly better in favour of the automatic tuning, in case of Demand Profile A. The manual tuning seems to be more efficient, with a reduced cost of control, in particular with Demand Profile B. This may be partially due to a small difference in the static gain of the two tunings. The results obtained with $F^3 PI$ allow instead to sensibly improve the cost of control at a very little price in term of regulation error, with respect to $F^1 PI$, as expected from the linear design. Moving to the results obtained with tunings characterised by $\omega_c^* = 0.03 \text{ rad/s}$, the metrics reported in Tables 11 and 12 suggest that $F^3 PI$ produces similar performances to those delivered by $F^1 PI$, as in Case Study A. Fig. 17 depicts the main signals for the simulation with $F^1 PI$.

8. Discussion of results

The analysis of results obtained in the regulator design phase, and presented in Section 6, highlights the ability of the optimisation based approach to deliver a wide range of reliable tunings. Moreover, the comparison with previously tuned regulators, further underlines the reliability of results. Finally, regulator structures with higher filter order can be useful to obtain improvements in both design objectives.

Results obtained in the regulator test phase, and presented in Section 7, suggest that the performances obtained with the automatic tuning procedure are aligned with those obtained with similar regulator designs, performed in a manual way and refined with trials on the nonlinear plant. Moreover, higher order filters may allow improving the results in more demanding situations, such as ω_c^* close to the

frequency region associated with resonance peaks. In less demanding situations, higher order filters may not allow to improve the actual results, despite the improvements introduced in the linear design framework. As already remarked in this paper, it is in fact more profitable to select a set of candidate tunings from the Pareto front (or fronts) since, due to the nonlinearity of the process under control, the results expected from the linear design may not be confirmed by tests on the plant. In this respect, it must be also remarked that the overall control approach proposed in Galuppini, Creaco et al. (2020) allows to reduce the risk of instability due to process nonlinearity, thus allowing performing more freely tests on the plant. A further remark concerns the fact that the optimisation-based tuning approach can be a useful tool also to design regulators based on transfer functions relating valve closure variation ($\delta\alpha(t) = \alpha(t) - \bar{\alpha}$) to the pressure variation ($\delta h(t)$). This may happen when the $\xi(\alpha)$ curve if the valve is not available. In this scenario, due to the strong gain nonlinearity characterising the process, it may be necessary to require much larger robustness margin than in the case of control based on $\xi(\alpha)$. To reduce conservatism, it may be more profitable to base the regulator design on a number of different models, approximating the system dynamics around different working points (Galuppini, Magni et al., 2020). A possibility is then modifying RT-BOOP to simultaneously consider different loop functions, resulting from the application of the same regulator to the different local process models. In particular, stability constraint (18) should be introduced for all loop functions, while robustness constraints (19)–(22) and objective functions J_1 and J_2 should consider worst case values. To conclude, the proposed bi-objective optimisation approach allows automatising the regulator tuning process, with no alteration of the original design rationale, while the solution of RT-BOOP by means of NSGA-II efficiently provides a wide range of possible tunings, with the guarantee that such tunings are optimal (or nearly so) in a Pareto sense. In this respect, the optimisation based procedure also allows for a better handling of the higher order regulator transfer functions described in Section 5.6, since, in this case, a profitable manual tuning of such regulators may become even more burdensome due to the high number of free design parameters.

9. Conclusion

This paper proposes a bi-objective optimisation approach for the regulator design, in the context of Real time pressure control in water distribution networks. The optimisation problem is based on a linear model that describes the process dynamics around a nominal working point, and encapsulates as constraints the fundamental requirements of closed loop stability and robustness. The two objective functions instead encode performance requirements related to process disturbance rejection and closed-loop settling time on one side, and deamplification of high frequency resonance peaks of the process and high frequency rejection on the other. The optimisation of both objective functions represents the typical design trade off in the shaping of sensitivity and complementary sensitivity function. The solution to the bi-objective optimisation problem is a Pareto front, where each solution represents an optimal combination of the two objective functions. The designer can take advantage from the knowledge of the whole front, by choosing the more suitable set of candidate tunings to be tested on the nonlinear plant, having a clear idea of the performance trade-off. The new approach is validated by comparing the new tunings with manual ones from previous works, and by performing a number of simulated experiments on two WDNs, under different demand scenarios. The new tuning process, carried out in the automatic way, results to be effective and efficient, while the performances delivered by the optimisation-based tunings are aligned with the expectations. Finally, the new approach also allows to handle more complex regulator structures, whose manual tuning may be difficult due to the high number of free design parameters. The use of more complex regulators allows to improve the design in the linear system framework, and may allow to

improve the performances of the control scheme, when tested on the nonlinear plant. A last remark concerns the generality of the proposed tuning approach. As a matter of fact, while the bi-objective tuning procedure is conceived for pressure control in WDNs in the context of this work, its characteristics make it an interesting tool in other fields of applications, in particular when it is important to balance between control performances and control sensitivity/robustness, but it may be difficult to have a clear idea of the actual, quantitative performances before having performed tests on the real plant.

Declaration of competing interest

The authors declare that they have no known competing financial interests or personal relationships that could have appeared to influence the work reported in this paper.

Appendix A. Robustness indicators

Consider a generic loop function $L(s)$. It is then possible to define the following robustness indicators (Magni & Scattolini, 2014):

- **Phase margin:** $\phi_m = 180^\circ - |\arg L(j\omega_c)|$, with ω_c s.t. $|L(j\omega_c)| = 1$, representing the maximum unmodelled delay admissible in the loop function that does not compromise asymptotic stability.
- **Gain margin:** $K_m = 1/|L(j\omega_\pi)|$, with ω_π s.t. $\arg(L(j\omega_\pi)) = -180^\circ$, representing the maximum unmodelled gain admissible in the loop function that does not compromise asymptotic stability.
- **Vector margin:** $\Delta_m = \min_{\omega} |1 + L(j\omega)|$, representing the minimum distance between the point -1 and the Nyquist plot of $L(s)$.

Note that phase and gain margins represent particular cases of the vector margin, which provides a more complete (but less intuitive) evaluation of the robustness of the control design.

Appendix B. Working points

For Case Study A, the working point WP_A is defined as follows:

$$WP_A = \begin{cases} \bar{\xi} = 871 \text{ (i.e. } \bar{\alpha} = 0.694) \\ \bar{H} = 50 \text{ m} \\ \bar{D}_1 = 0.1 \text{ m}^3/\text{s} \\ \bar{h} = 29 \text{ m} \\ \bar{Q} = 0.1 \text{ m}^3/\text{s} \end{cases} \quad (38)$$

For Case Study B, the working point WP_B is defined as follows:

$$WP_B = \begin{cases} \bar{\xi} = 170.45 \text{ (i.e. } \bar{\alpha} = 0.619) \\ \bar{H} = 39.6 \text{ m} \\ \bar{D}_1 = 0.0014 \text{ m}^3/\text{s} \\ \dots \\ \bar{D}_{N_{nodes}} = 0.0007 \text{ m}^3/\text{s} \\ \bar{h} = 25 \text{ m} \\ \bar{Q} = 0.0586 \text{ m}^3/\text{s} \end{cases} \quad (39)$$

Recall that the average value of each demand $D_i(t)$ is the same for demand profiles A and B, therefore a single working point WP_B can be defined for Case Study B.

Finally, note that, for both case studies, the WP are the same adopted in Galuppini, Creaco et al. (2020), for sake of comparison.

Appendix C. Gain scheduling

To compensate for the dependence of the process static gain on the square of the flow Q , the regulator gain can be adjusted by computing, at each time instant, the adapted regulator gain $\mu_r^{g_{sq}}(t)$, as follows:

$$\mu_r^{g_{sq}}(t) = \mu_r \left(\frac{\bar{Q}}{Q(t)} \right)^2 \quad (40)$$

with μ_r the nominal regulator static gain.

Similarly, the Smith Predictor can be adjusted by adapting, at each time instant, the gain of $G'(s)$.

Moreover, to reduce the control effort associated with valve operation at very open positions, it is possible to modify Eq. (40) to introduce a multiplicative factor $\mu_{ratio}(\alpha(t))$ depending on α , and compute the adapted regulator gain $\mu_r^{g_{sa}}(t)$, at each time instant, as follows:

$$\mu_r^{g_{sa}}(t) = \mu_{ratio}(\alpha(t))(\mu_r^{g_{sq}}(t)) \quad (41)$$

with $\mu_{ratio}(\alpha(t)) \in (0, 1]$.

Note that, for sake of comparison with results from Galuppini, Creaco et al. (2020), the same $\mu_{ratio}(\alpha(t))$ is adopted for $GS - \alpha$:

$$\mu_{ratio}(\alpha(t)) = \begin{cases} 1 & \forall \alpha(t) > \alpha^* \\ k * \alpha^{*p} + \mu_{ratio}^* & \forall \alpha(t) \leq \alpha^* \end{cases} \quad (42)$$

$$k = \frac{1 - \mu_{ratio}^*}{\alpha^{*p}}; \quad (43)$$

with $\alpha^* \in [0; 1]$, $\mu_{ratio}^* \in (0; 1]$ and $p > 0$ free design parameters.

For Case Study A and tunings characterised by $\omega_c^* = 0.05$ rad/s, the parameters of the gain scheduling policy $GS - \alpha$ are the following:

$$\alpha^* = 0.55 \quad (44)$$

$$\mu_{ratio}^* = 0.1 \quad (45)$$

$$p = 4 \quad (46)$$

For tunings characterised by $\omega_c^* = 0.01$ rad/s, $GS - \alpha$ is not active.

For Case Study B and tunings characterised by $\omega_c^* = 0.03$ rad/s, the parameters of the gain scheduling policy $GS - \alpha$ are the following:

$$\alpha^* = 0.5 \quad (47)$$

$$\mu_{ratio}^* = 0.1 \quad (48)$$

$$p = 6 \quad (49)$$

For tunings characterised by $\omega_c^* = 0.01$ rad/s, $GS - \alpha$ is not active.

References

- Alvisi, S., Franchini, M., & Luciani, C. (2018). Application of water consumption smart metering for water loss assessment: a case study. In *WDSA/CCWI joint conference proceedings*, vol. 1.
- Avvedimento, S., Todeschini, S., Giudicianni, C., Di Nardo, A., Walski, T., & Creaco, E. (2020). Modulating nodal outflows to guarantee sufficient disinfectant residuals in water distribution networks. *Journal of Water Resources Planning and Management*, 146(8), Article 04020066.
- Campisano, A., Creaco, E., & Modica, C. (2009). Rtc of valves for leakage reduction in water supply networks. *Journal of Water Resources Planning and Management*, 136(1), 138–141.
- Campisano, A., Modica, C., Reitano, S., Ugarelli, R., & Bagherian, S. (2016). Field-oriented methodology for real-time pressure control to reduce leakage in water distribution networks. *Journal of Water Resources Planning and Management*, 142(12), Article 04016057.
- Campisano, A., Modica, C., & Vetrano, L. (2011). Calibration of proportional controllers for the rtc of pressures to reduce leakage in water distribution networks. *Journal of Water Resources Planning and Management*, 138(4), 377–384.
- Candelieri, A., & Archetti, F. (2014). Smart water in urban distribution networks: limited financial capacity and big data analytics. *WIT Transactions on The Built Environment*, 139.
- Cembrano, G., Wells, G., Quevedo, J., Pérez, R., & Argelaguet, R. (2000). Optimal control of a water distribution network in a supervisory control system. *Control Engineering Practice*, 8(10), 1177–1188.

- Ciaponi, C., Franchioli, L., Murari, E., & Papiri, S. (2015). Procedure for defining a pressure-outflow relationship regarding indoor demands in pressure-driven analysis of water distribution networks. *Water Resources Management*, 29(3), 817–832.
- Cominos, P., & Munro, N. (2002). Pid controllers: recent tuning methods and design to specification. *IEE Proceedings D (Control Theory and Applications)*, 149(1), 46–53.
- Creaco, E. (2017). Exploring numerically the benefits of water discharge prediction for the remote rte of wdns. *Water*, 9(12), 961.
- Creaco, E., Campisano, A., Fontana, N., Marini, G., Page, P., & Walski, T. (2019). Real time control of water distribution networks: a state-of-the-art review. *Water Research*.
- Creaco, E., Campisano, A., Franchini, M., & Modica, C. (2017). Unsteady flow modeling of pressure real-time control in water distribution networks. *Journal of Water Resources Planning and Management*, 143(9), Article 04017056.
- Creaco, E., Campisano, A., & Modica, C. (2018). Testing behavior and effects of prvs and rte valves during hydrant activation scenarios. *Urban Water Journal*, 15(3), 218–226.
- Creaco, E., & Walski, T. (2017). Economic analysis of pressure control for leakage and pipe burst reduction. *Journal of Water Resources Planning and Management*, 143(12), Article 04017074.
- de Winter, C., Palletti, V. R., Worm, D., & Kooij, R. (2019). Optimal placement of imperfect water quality sensors in water distribution networks. *Computers & Chemical Engineering*, 121, 200–211.
- Deb, K. (2001). *Multi-objective optimization using evolutionary algorithms*, Vol. 16. John Wiley & Sons.
- Deb, K., Pratap, A., Agarwal, S., & Meyarivan, T. (2002). A fast and elitist multiobjective genetic algorithm: Nsga-ii. *IEEE Transactions on Evolutionary Computation*, 6(2), 182–197.
- Farley, M., & Trow, S. (2003). *Losses in water distribution networks*. IWA publishing.
- Fiorillo, D., Creaco, E., De Paola, F., & Giugni, M. (2020). Comparison of bottom-up and top-down procedures for water demand reconstruction. *Water*, 12(3), 922.
- Fiorillo, D., Galuppini, G., Creaco, E., De Paola, F., & Giugni, M. (2020). Identification of influential user locations for smart meter installation to reconstruct the urban demand pattern. *Journal of Water Resources Planning and Management*, 146(8), Article 04020070.
- Fontana, N., Giugni, M., Glielmo, L., & Marini, G. (2016). Real time control of a prototype for pressure regulation and energy production in water distribution networks. *Journal of Water Resources Planning and Management*, 142(7), Article 04016015.
- Fontana, N., Giugni, M., Glielmo, L., Marini, G., & Verrilli, F. (2017). Real-time control of a prv in water distribution networks for pressure regulation: Theoretical framework and laboratory experiments. *Journal of Water Resources Planning and Management*, 144(1), Article 04017075.
- Fontana, N., Giugni, M., Glielmo, L., Marini, G., & Zollo, R. (2017). Real-time control of pressure for leakage reduction in water distribution network: Field experiments. *Journal of Water Resources Planning and Management*, 144(3), Article 04017096.
- Fontana, N., Giugni, M., Glielmo, L., Marini, G., & Zollo, R. (2020). Use of hydraulically operated prvs for pressure regulation and power generation in water distribution networks. *Journal of Water Resources Planning and Management*, 146(7), Article 04020047.
- Fontana, N., Giugni, M., & Portolano, D. (2012). Losses reduction and energy production in water-distribution networks. *Journal of Water Resources Planning and Management*, 138(3), 237–244.
- Gaikwad, S., Dash, S., & Stein, G. (1999). Auto-tuning pid using loop-shaping ideas. In *Proceedings of the 1999 IEEE International conference on control applications (Cat. No. 99CH36328)*, vol. 1 (pp. 589–593). IEEE.
- Galuppini, Giacomo, Creaco, Enrico, & Magni, Lalo (2020). A gain scheduling approach to improve pressure control in water distribution networks. *Control Engineering Practice*, 103, 104612.
- Galuppini, G., Creaco, E., Toffanin, C., & Magni, L. (2019). Service pressure regulation in water distribution networks. *Control Engineering Practice*, 86, 70–84.
- Galuppini, G., Magni, L., & Creaco, E. (2020). Stability and robustness of real-time pressure control in water distribution systems. *Journal of Hydraulic Engineering*, 146(4), Article 04020023.
- Grassi, E., & Tsakalis, K. (1996). Pid controller tuning by frequency loop-shaping. In *Proceedings of 35th IEEE conference on decision and control*, vol. 4 (pp. 4776–4781). IEEE.
- Grosso, J. M., Maestre, J. M., Ocampo-Martinez, C., & Puig, V. (2014). On the assessment of tree-based and chance-constrained predictive control approaches applied to drinking water networks. *IFAC Proceedings Volumes*, 47(3), 6240–6245, 19th IFAC World Congress.
- Grosso, J., Ocampo-Martinez, C., Puig, V., & Joseph, B. (2014). Chance-constrained model predictive control for drinking water networks. *Journal of Process Control*, 24(5), 504–516.
- Grosso, J. M., Velarde, P., Ocampo-Martinez, C., Maestre, J. M., & Puig, V. (2017). Stochastic model predictive control approaches applied to drinking water networks. *Optimal Control Applications & Methods*, 38(4), 541–558.
- Hermann, M., Pentek, T., & Otto, B. (2016). Design principles for industrie 4.0 scenarios. In *2016 49th Hawaii international conference on system sciences (HICSS)* (pp. 3928–3937). IEEE.
- Janus, T., & Ulanicki, B. (2017). *Hydraulic Modelling for Pressure Reducing Valve Controller Design Addressing Disturbance Rejection and Stability Properties*. Elsevier.
- Janus, T., & Ulanicki, B. (2018). Improving stability of electronically controlled pressure-reducing valves through gain compensation. *Journal of Hydraulic Engineering*, 144(8), Article 04018053.
- Jiménez-Cabas, J., Romero-Fandiño, E., Torres, L., Sanjuan, M., & López-Estrada, F. R. (2018). Localization of leaks in water distribution networks using flow readings. *IFAC-PapersOnLine*, 51(24), 922–928.
- Kauffeld, I. (2018). *An algorithm for placing sensors ensuring fault detection and isolation in water distribution networks* (Ph.D. thesis).
- Lambert, A., Fantozzi, M., & Thornton, J. (2013). Practical approaches to modeling leakage and pressure management in distribution systems—progress since 2005. In *Proceedings of the 12th int. conf. on computing and control for the water industry-CCWI2013*, 2013.
- Magni, L., & Scattolini, R. (2014). *Advanced and multivariable control*. Pitagora.
- Mennemann, J.-F., Marko, L., Schmidt, J., Kemmetmüller, W., & Kugi, A. (2019). Nonlinear model predictive control of a variable-speed pumped-storage power plant. *IEEE Transactions on Control Systems Technology*.
- Ocampo-Martinez, C., Barcelli, D., Puig, V., & Bemporad, A. (2012). Hierarchical and decentralised model predictive control of drinking water networks: Application to barcelona case study. *IET Control Theory & Applications*, 6(1), 62–71.
- Ocampo-Martinez, C., Puig, V., Cembrano, G., & Quevedo, J. (2013). Application of predictive control strategies to the management of complex networks in the urban water cycle [applications of control]. *IEEE Control Systems*, 33(1), 15–41.
- Pezzinga, G. (2000). Evaluation of unsteady flow resistances by quasi-2d or 1d models. *Journal of Hydraulic Engineering*, 126(10), 778–785.
- Pugliese, F., De Paola, F., Fontana, N., Giugni, M., & Marini, G. (2016). Experimental characterization of two pumps as turbines for hydropower generation. *Renewable energy*, 99, 180–187.
- Salomons, E., & Housh, M. (2020). A practical optimization scheme for real-time operation of water distribution systems. *Journal of Water Resources Planning and Management*, 146(4), Article 04020016.
- Seborg, D. E., Mellichamp, D. A., Edgar, T. F., & Doyle, F. J., III (2010). *Process dynamics and control*. John Wiley & Sons.
- Sedlak, D. (2014). *Water 4.0: The past, present, and future of the world's most vital resource*. Yale University Press.
- Streeter, V. L., Wylie, E. B., & Bedford, K. W. (1998). *Fluid mechanics*, wcb.
- Tan, W., Liu, J., & Tam, P. (1998). Pid tuning based on loop-shaping h_∞ control. *IEEE Proceedings D (Control Theory and Applications)*, 145(6), 485–490.
- Thornton, J., & Lambert, A. (2006). Managing pressures to reduce new breaks. *Water*, 21(2006), 24–26.
- Toro, R., Ocampo-Martinez, C., Logist, F., Impe, J. V., & Puig, V. (2011). Tuning of predictive controllers for drinking water networked systems. *IFAC Proceedings Volumes*, 44(1), 14507–14512, 18th IFAC World Congress.
- Van Zyl, J., & Cassa, A. (2013). Modeling elastically deforming leaks in water distribution pipes. *Journal of Hydraulic Engineering*, 140(2), 182–189.